FINITE ELEMENT ANALYSIS OF BEAM-TO-BEAM ECCENTRIC END PLATE CONNECTIONS

EŞ EKSENLİ KİRİŞ BAĞLANTILARININ SONLU ELEMANLAR YÖNTEMİ İLE ANALİZİ

SAMET ELTAŞ

PROF. DR. BORA YILDIRIM

Supervisor

PROF. DR. MEHMET ALİ GÜLER

2nd Supervisor

Submitted to

Graduate School of Science and Engineering of Hacettepe University

as a Partial Fulfillment to the Requirements

for the Award of the Degree of Master of Science

in Mechanical Engineering

June 2023

ABSTRACT

FINITE ELEMENT ANALYSIS OF BEAM-TO-BEAM ECCENTRIC END PLATE CONNECTIONS

Samet Eltaş

Master of Science, Mechanical Engineering

Supervisor: Prof. Dr. Bora Yıldırım

2nd Supervisor: Prof. Dr. Mehmet Ali Güler

June 2023, 60 pages

This study presents a broad investigation on eccentric end plates used for beam-to-beam connections by utilizing finite element analysis. This investigation is based on previous experimental work on beam-to-beam connections conducted by a supervisor of this thesis. These connections are vitally essential in the modeling of lightweight structures. For beam to beam joints, there are numerous varieties of joints, including shear plate, clip angle joint, and eccentric end plate, along with T-stub joints, that are frequently used in frame structures. Understanding the rotational attitude of the joints is a fundamental aspect of design. A practical way of evaluating their response is to generate moment-rotation curves and investigate the effects of several parameters graphically. It is concluded that the stiffeners and the end plate are the critical components for failure.

Keywords: Parametric study using FEA, beam-to-beam connections, semi rigid steel joints, eccentric end plate connections

ÖZET

EŞ EKSENLİ KİRİŞ BAĞLANTILARININ SONLU ELEMANLAR YÖNTEMİ İLE ANALİZİ

Samet Eltaş

Yüksek Lisans, Makine Mühendisliği

Danışman: Prof. Dr. Bora Yıldırım

Eş Danışman: Prof. Dr. Mehmet Ali Güler

Mart 2023, 60 sayfa

Kiriş-kiriş bağlantıları, T-stub, eş eksen plakası, kesme plakası, ek plakaların kullanıldığı bağlantılar gibi pek çok farklı konfigürasyonda yapılabilmektedir. Söz konusu bağlantı tipleri arasında eş eksen plakaları son dönemlerde önem kazanmaya başlamıştır. Özellikle geniş tabanlı yapılarda ve konstrüksiyonun zorunlu kıldığı yerlerde eş eksenli kiriş bağlantı tipini kullanmak kaçınılmaz olmuştur. Bu çalışma eş eksenli kiriş bağlantıları üzerine sonlu elemanlar analizi yöntemini kullanarak geniş bir araştırma sunmaktadır. Bağlantıların yapısal yüklere verdiği cevapları anlamanın ve bu cevaplara göre uygun dayanım sınıflandırmalarının yapılabilmesinin en pratik yolu moment-rotasyon grafiklerinin elde edilmesidir. Bu çalışma bir dizi parametrenin değiştirilmesi ile eş eksen kiriş bağlantılarının davranış biçimlerini incelemiş ve dayanım sınıflandırmalarını sunmuştur.

Keywords: Kiriş-kiriş bağlantıları, eş eksenli plaka bağlantıları, sonlu elemanlar yöntemiyle parametrik çalışma, yarı rijid çelik bağlantılar

CONTENTS

Page

TABLES

FIGURES

1. INTRODUCTION

Generally, primary beams are utilized to connect spaces between frame columns. The secondary beams, on the other hand, are united to primary beams to enhance distribution of floor burdens and reinforce the slabs.

These beams are joined in a frame construction utilizing welded or bolted connections. The frame construction is completed by these connections, which can either be single-sided or double-sided in arrangement [3].

For beam-to-beam connections, several kinds of joints are available, including shear plate, clip angle joints, eccentric end plate, connections using additional plates, T-stub, and top seat angle joints [4–8]. In the structural steel market, end-plate connections have attracted substantial attention due to the low price, simplicity of manufacturing, and ease of installation, particularly when complicated architectural structures are required.

While the literature has several investigation on beam-to-column connections, very limited investigations are available about beam to beam connections. This is one of the fewer published investigations on this connection type, Lopez et al. [9] analyzed a non-standard component known as "extra plate in bending" that used for beam-to-beam connection and developed a theoretical description of the connection via experimental, and computational research. Finding is that suggested extra plate exposed to bending serves as the most significant contributor to the stiffness, and the rigidity of the structure. Using the component technique and numerical analysis, Urbanos et al. [10] examined tension, compression, and bending effects on beam to beam bolted end plate connections. If considerable axial forces are exerted on the joint, they proposed that this design comprise the cumulative influence of the axial and bending forces. Natesan et al. [11] studied the two distinct beam to beam connection configurations' characteristic. First sort of connection between the two beams is a clip angle connection, second one is the flange strip joint. Distortion buckling and local buckling are found in the first case, though pullout failure was detected for second case. Mohamadi-Shooreh et al. [12] provided a new predicted experimental model. Regarding

moment-rotation behavior, they suggested an equation utilizing an exponential function that may provide satisfactory results. Experimentally examining three alternative beam-to-beam connections (EEP, PDEP, FP), Hawxwell and Tsavdaridis [2] determined that eccentric end plate connection showed stiffer behavior than other joints, thus classified it in semi-rigid category.

1.1. Scope Of The Thesis

As a continuation of Hawxwell and Tsavdaridis' experimental work [2], this study offers a thorough understanding of EEP connections with changing parameters. Using the experimental results presented in [2], a numerical model is constructed and validated. As a result, this study presents an in-depth analysis of influences of various parameters, such as the stiffeners along with end plates' thicknesses, length and section size of beams, and height level variations of end plates, on the characteristics of beam-to-beam EEP connections. Additionally, impact of two distinct end plate types on joint characteristic is examined. Finally, impact of the eliminating some bolts on connection's rigidity is investigated.

1.2. Contributions

Although EN-1993-Part 1-8 [13] covers joints that transfer bending moments, beam-to-beam fixed connections are not standardized, which frequently leads to doubts about the reliability of their rotational capacity. Following experimental tests, this investigation presents a thorough investigation on the eccentric end plate connections between beams using finite element technique. To offer a trustworthy analytical model on the structural characteristic under monotonic vertical loading, a parametric study is carried out using experimental data. An adequate rotational stiffness and moment capacity were displayed by the eccentric end plate connection. For a more accurate assessment of critical factors affecting the stability of connection, failure mechanism of the connection's components is also described. Finally, this study may continue by look into the application of cyclic loading protocols using standard or prestressed bolts in the future.

2. BACKGROUND OVERVIEW

In designing and analyzing steel structures, connections are typically depicted as either rigid or flexible. According to the flexible connection presumption, moment transmission does not exist between the connected members. In contrast, the acceptance of rigid connection states that there will be no rotation among the joint elements. Those simplified acceptations are simple to use, however typically fail to precisely represent the structure's mechanics [14–17]. Findings of the research studies in this context show that most of the connections fall between these two extremes in real life and called as semi-rigid connections [18–23]. Moreover, by modeling the connections as semi-rigid, the input loads in the connecting members can dissipate at the joint which improves both static and seismic resistance of the structure [24]. Therefore, a comprehensive understanding of characteristic of steel structure connections is necessary to model safe and cost-effective frame structures. The most common way of modeling these joints including the true physics behind them is to obtain validated moment-rotation curves belonging to these connections. These curves gives ideas about two key characteristics: rotational stiffness and rotation capacity [25]. A well-designed joint should meet the required strength, rigidity and ductility to provide moment-resisting frames [26].

2.1. Classification of steel connections

There are three varieties of connections in Eurocode 3: rigid, semi rigid, flexible. A simple classification of the joints depicted as a graph in Fig. 2.1 in terms of the connection rigidity. In order to investigate a structure general behavior, moments within a structure, deformations of the structure and effects of the connections on transmitting internal forces between joint parts should be taken into account. When it comes to joint behavior, the three connection types mentioned above exhibit different characteristics. Thus, the appropriate joint type should be determined in order to make sensible assessments.

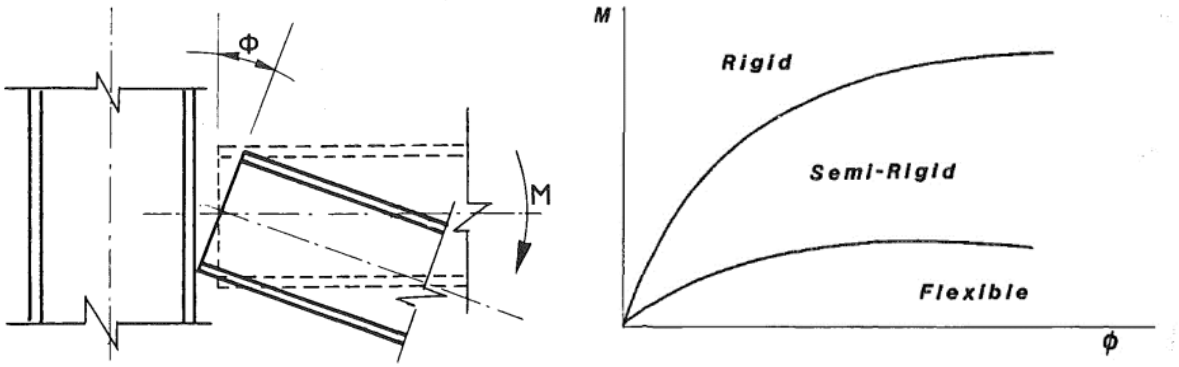

Figure 2.1 Boundary conditions and applied load

i) Rigid Connections

This is a continuous joint in which the structure behaves as there is a continuity between the connecting parts. These connections have adequate rotational stiffness which allow perform analysis base upon full continuity method.

ii) Semi-Rigid Connections

Semi-rigid connections transmit both the internal forces and the internal moments. This connection type is as a transition between the flexible joints and rigid joints. The design moment rotation characteristics of connections can be utilized to predict their behavior. Thus, their behavior must be reflected into analysis as correct as possible.

iii) Nominally Pinned (Flexible) Connections

Nominally pinned joints transfer internal forces between the connected parts whereas do not transmit bending moments that much.

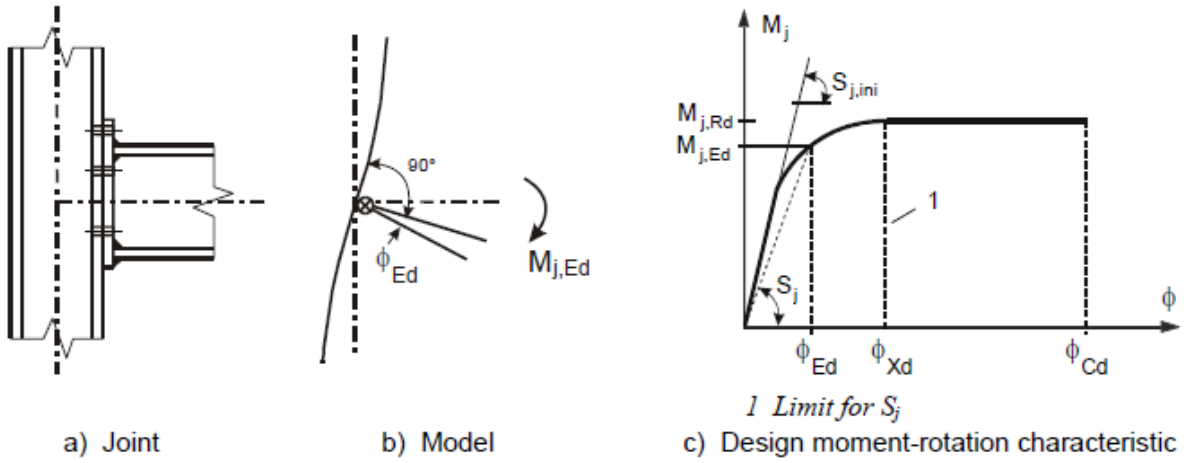

Figure 2.2 Boundary conditions and applied load

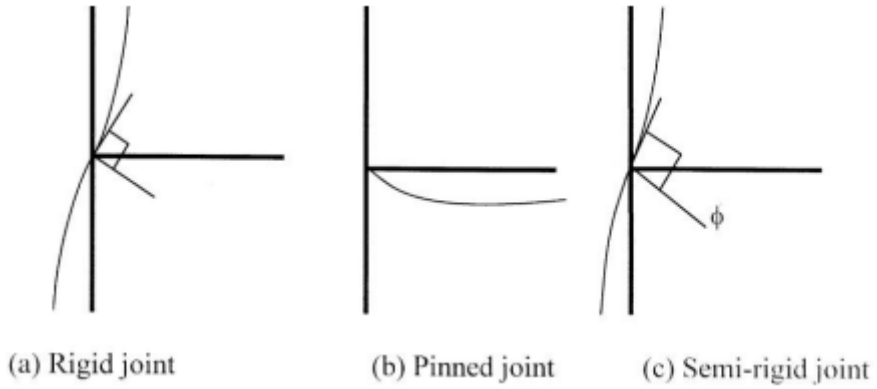

Figure 2.3 Joint classification based on rotational stiffness [1]

3. THE EXPERIMENT AND THE FE MODEL

The FE model was constructed using ANSYS software and includes all the necessary components, such as the primary beam, secondary beam, and all the connecting plates. The static analysis findings are in excellent accord with the experimental results, validating the FE model's precision. Figure 3.1 illustrates the monotonic loading's direction and location.

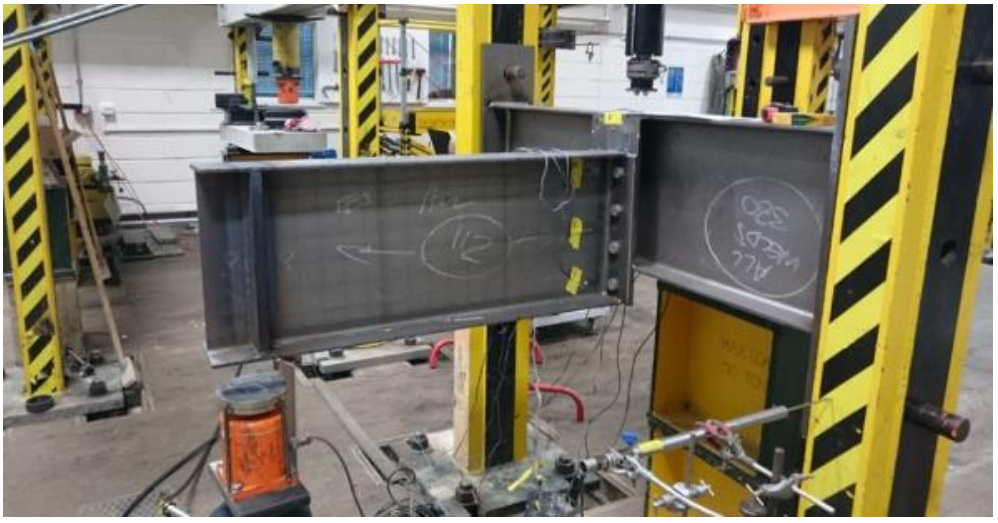

(a)

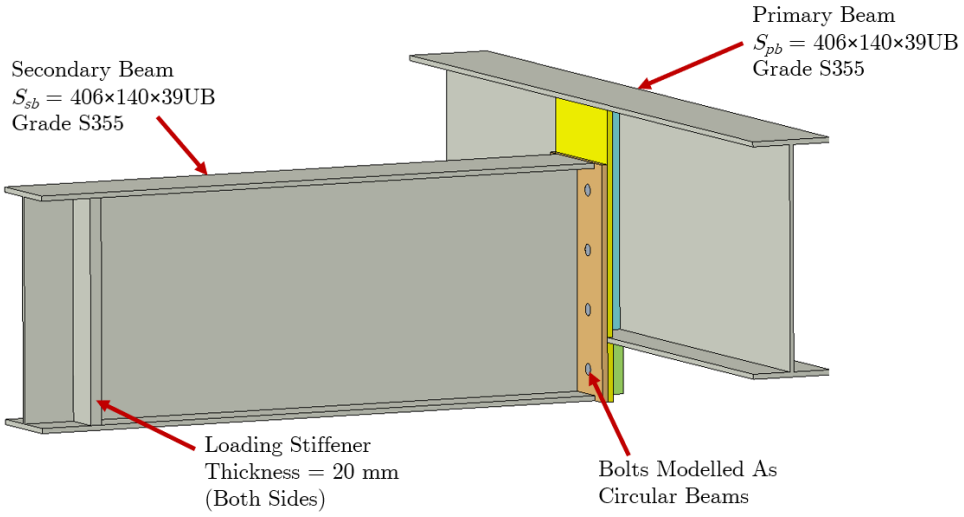

(b)

Figure 3.1 Illustration of main geometry a) experiment [2] b) 3D model

4. FEA PREPARATION of THE EEP CONNECTION

In the subsequent part, FE model of base structure is described.

4.1. Model Geometry

A primary and a secondary beams are two fundamental components which made up the architecture. Primary beam is responsible for carrying the majority of the load, while the secondary beam provides additional support and stability. The connecting elements are designed to transfer forces between the two beams and ensure a strong and durable connection. Figure 4.1 depicts the 3D solid representation of EEP connection. Figure 3.1 depicts the experimental setup and 3D model as well. Figure 4.2 illustrates the connecting members' specifics.

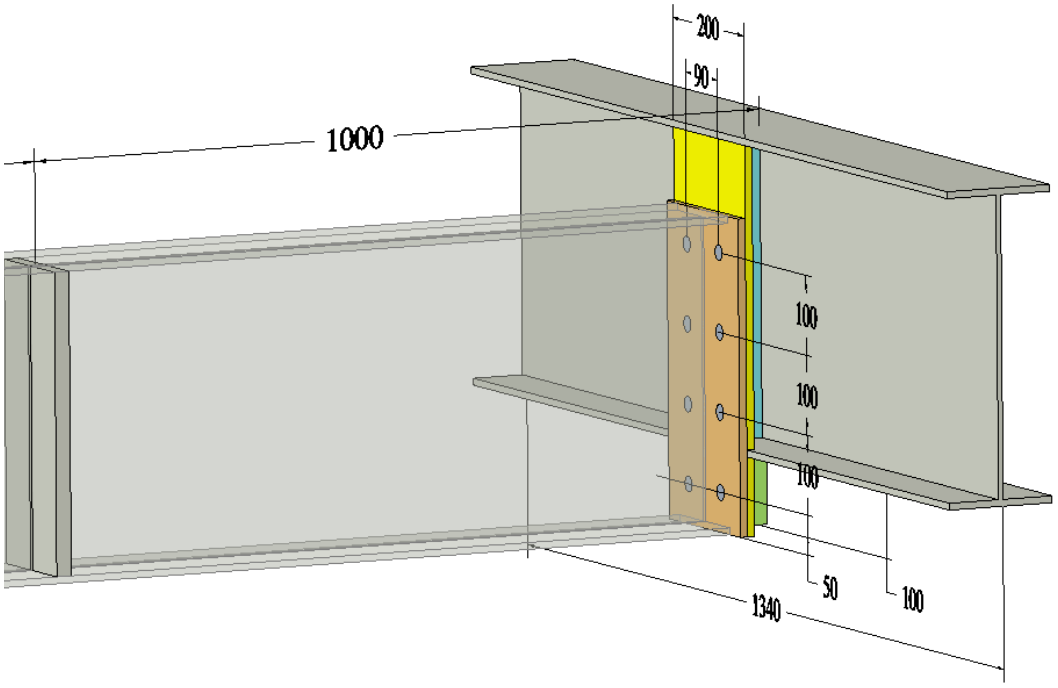

Figure 4.1 EEP connection's dimensions

The geometry includes two fundamental components, namely, a primary beam, a secondary beam and connection members as shown above.

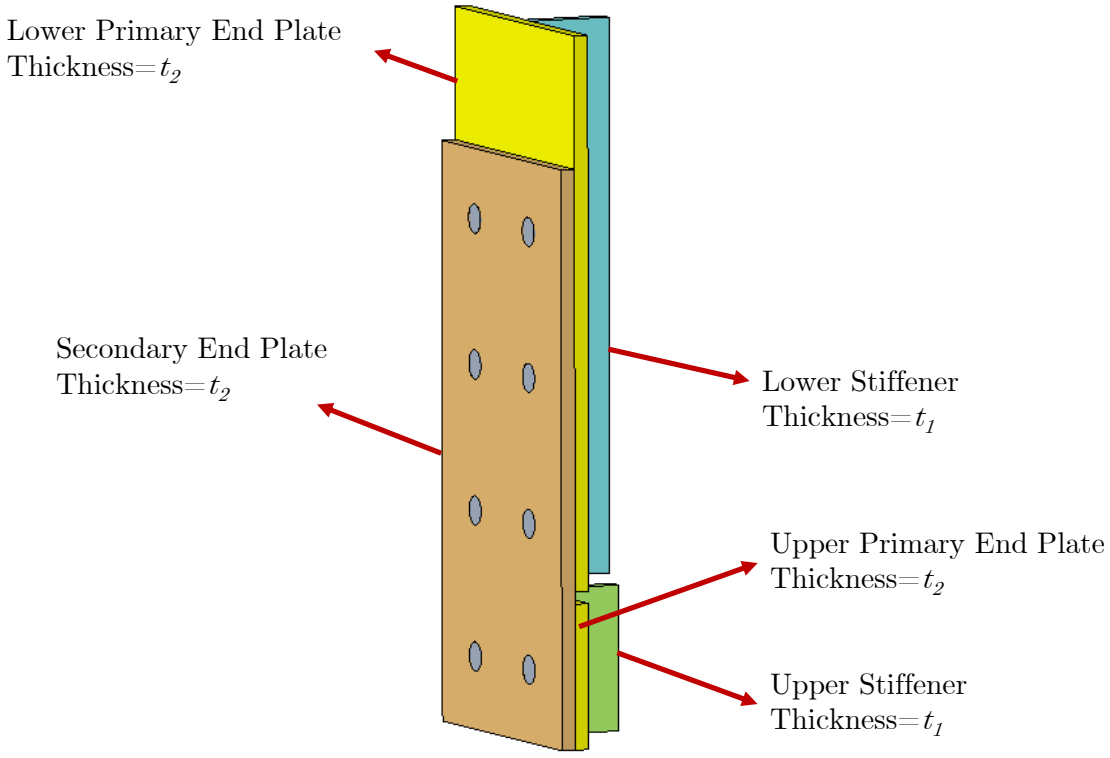

Figure 4.2 3D illustration of the EEP joint parts

Stiffeners' thickness for the base model are $t_1 = 10$ mm, while end plates' thicknesses are $t_2 = 10$ mm. Section sizes of the both beams are 406×140×39UB, and the steel used is grade S355. As can be seen in figure above secondary end plate end primary end plate are not flush to each other. Thus, connected beams are moved away from one another by 100 mm (-z). Bolts are grade 8.8 M20.

4.2. Material Properties

Except bolts, all parts are made of S355 steel. For all steel parts and bolts, a bi-linear isotropic hardening material model is established. The experimental investigation of Ref. [2] provided the material characteristics that are given in Table 4.1 for the steel parts and bolts. For all components, the Poisson's ratio taken as 0.3.

Table 4.1 Material Properties

Parts	**Material Properties**			
	f_y **[MPa]**	f_u **[MPa]**	**Elastic Modulus [GPa]**	**Tangent Modulus [MPa]**
S355 Steel	391	528	180	5200
M20, Grade 8.8 Bolt	650	810	180	700

4.3. FE bolt modeling

The circular bolt geometry is modeled utilizing the BEAM188 ANSYS element type, which gives the option to forego using any solid element description. So, it can be defined as a line element consist of two nodes at each end constructs the circular beam. Multi-point constraints (MPCs) are used to link the pilot nodes which named I and J to the multi-point constraints in Fig. 4.3 that show the heads of the bolts and nuts.

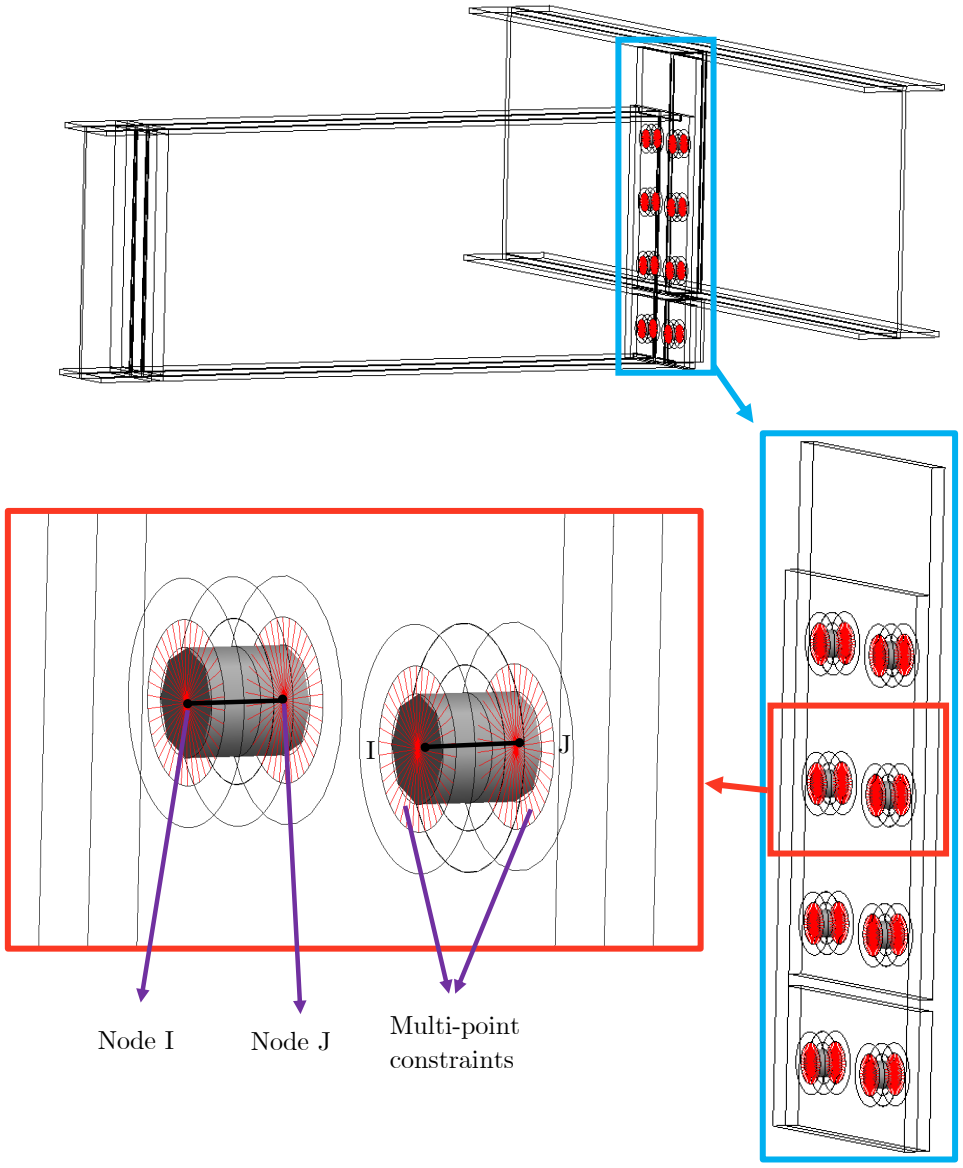

Figure 4.3 FE modeling of the bolts

4.4. Boundary Conditions

End plates are used at both end of primary beam to link it to the test column in the test setup. According to Fig. 4.4, both ends of primary beam are assumed rigid so, as a result, limited in

every directions. It can be seen that in Fig. 4.4, the loading placed across the load stiffeners in sub-steps, 1000 mm far away from the center of primary beam.

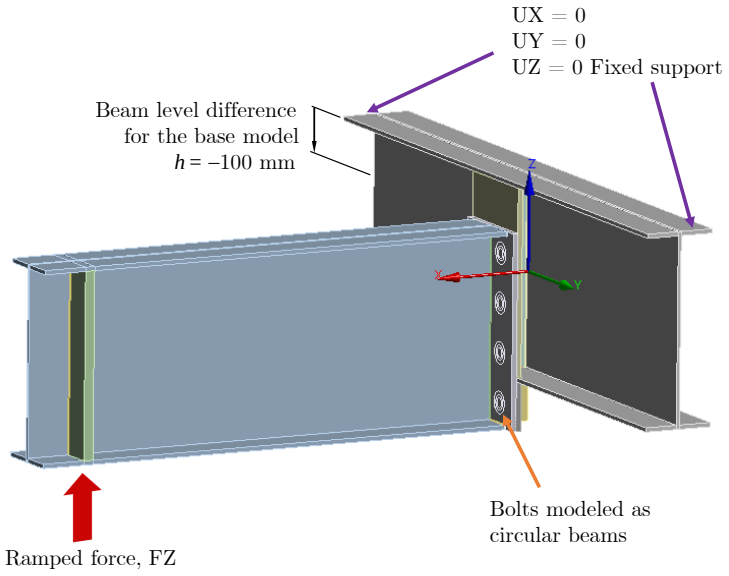

Figure 4.4 Boundary conditions and applied load

From zero up to a value at which a joint detail component fails which means observing 528 MPa, loading is delivered as a linear rising force. This indicates that each final instant value reflects the strength potential of the related joint. Once the UTS is found in any component, the analysis is assumed to be complete. The loading area is equal to 2,836 mm2, which equals to multiplication of the beam's width (141.8 mm) and stiffener's thickness (20 mm).

4.5. Beam Rotation Calculation

Three LVDT gauges are employed in the tests described in [2] to monitor the deflections. Primary beam's rotation is measured by two LVDT gauges that are placed 300 mm apart on the rear of the primary beam back.

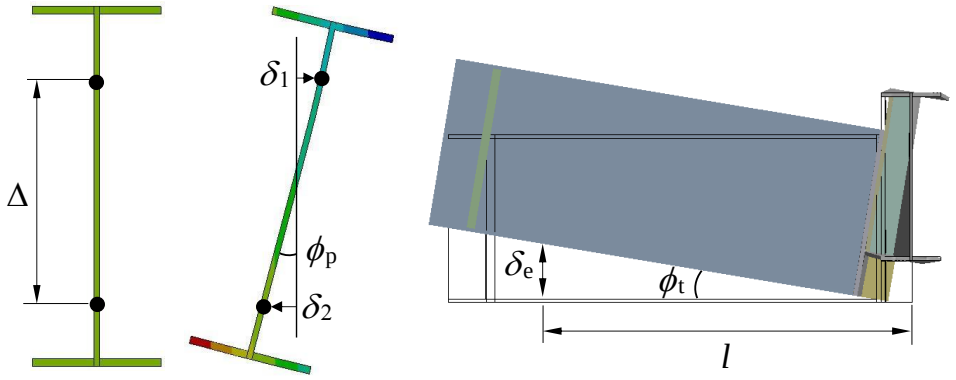

Figure 4.5 Calculation of the beam rotation

In Fig. 4.5, the deformations related to these LVDTs are denoted as δ_1 and δ_2. To measure end deflection δ_e, the last LVDT is positioned $l = 850$ mm far away from primary beam web's centerline. Primary beam's rotation, ϕ_p, and secondary beam's rotation, ϕ_s are calculated using following equations.

$$\phi_p = \frac{\delta_2 - \delta_1}{\Delta}, \tag{1}$$

$$\phi_s = \phi_t - \phi_p, \tag{2}$$

where

$$\phi_t = \frac{\delta_e}{l}, \tag{3}$$

denotes overall rotation of connection and $\Delta = 300$ mm.

4.6. Finite Element Mesh

Figure 4.6 depicts the FE mesh used to model the structure.

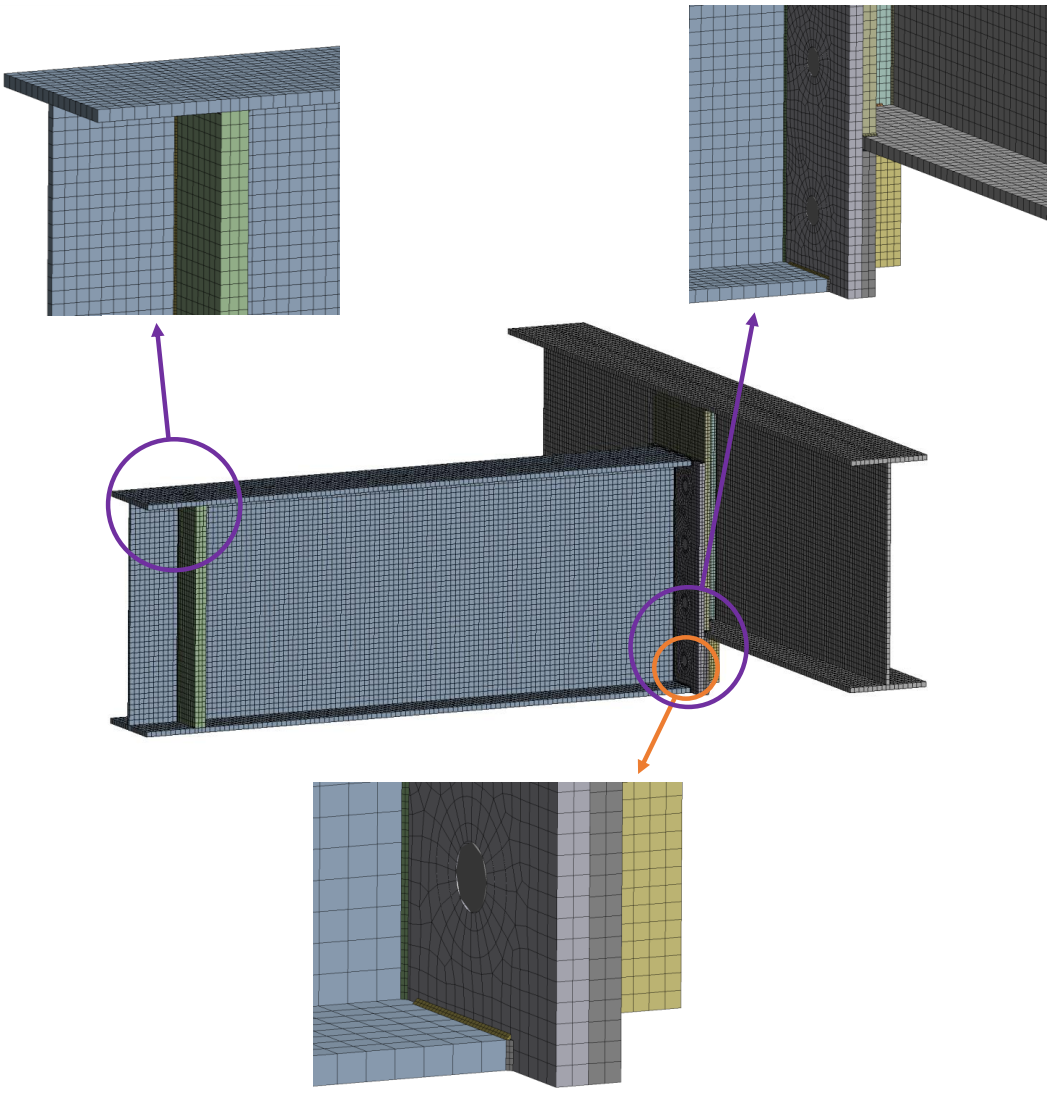

Figure 4.6 Mesh view

The ANSYS library's SOLID186 element type is used to mesh each component. To decide use which type of element, a comparison study is conducted. Findings show the quadratic elements provide more precise outcomes than the linear elements. The comparison of the findings for the load vs. end deflection and moment vs. rotation is shown in Fig. 4.7.

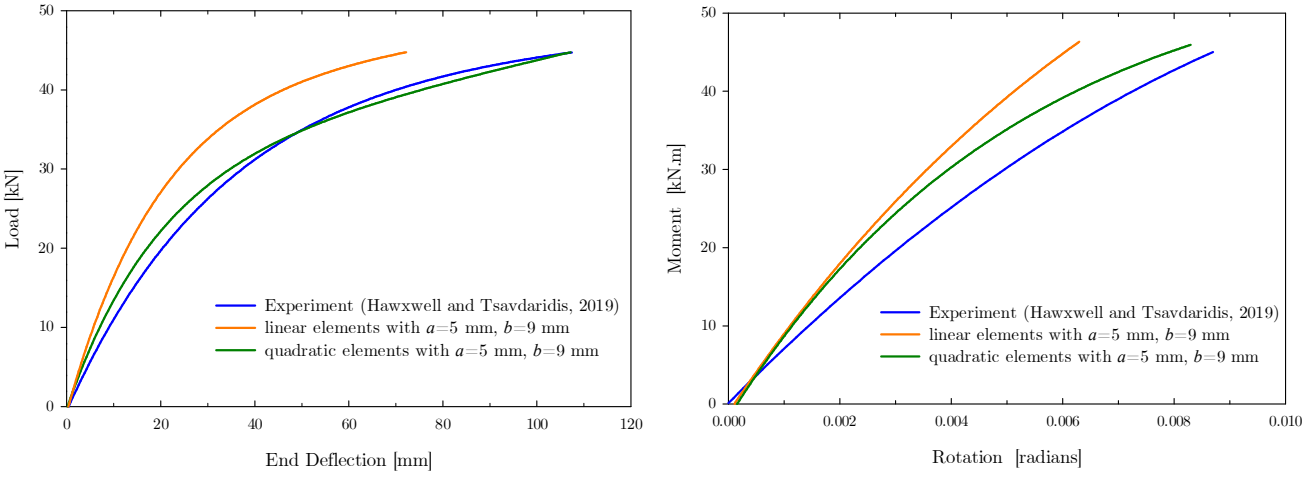

Figure 4.7 Element types effect

4.7. Contact Definitions

The FE model classifies contact surfaces into two distinct categories: frictional contact and bonded contact. For the individual parts that interact directly, frictional contact is used. Bonded contact is only defined for welding surfaces, so component surfaces must be in bonded contact with the welds. In a sensitivity analysis, the friction coefficient used in frictional contact is altered from 0.1 to 0.4 to see if it has a noticeable effect. As the friction coefficients chosen within this realistic range do not substantially influence the results (see Fig. 4.8), it is determined that the expected median of the range value will be 0.2. The CONTA174 and TARGE170 element categories are used to define contacts.

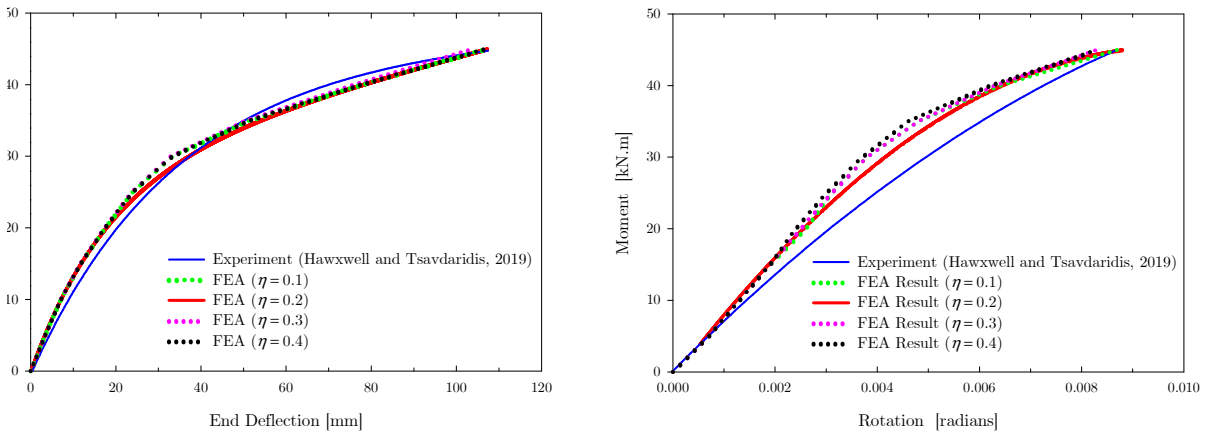

Figure 4.8 Effect of friction coefficient, η [2]

4.8. Mesh Convergence Study

According to Fig. 4.9, there are two different mesh sizes, a and b, for connection parts and other components. At the vicinity of joint locations where it is anticipated that critical stress and strain gradients will occur, a finer mesh size is utilized as in [27].

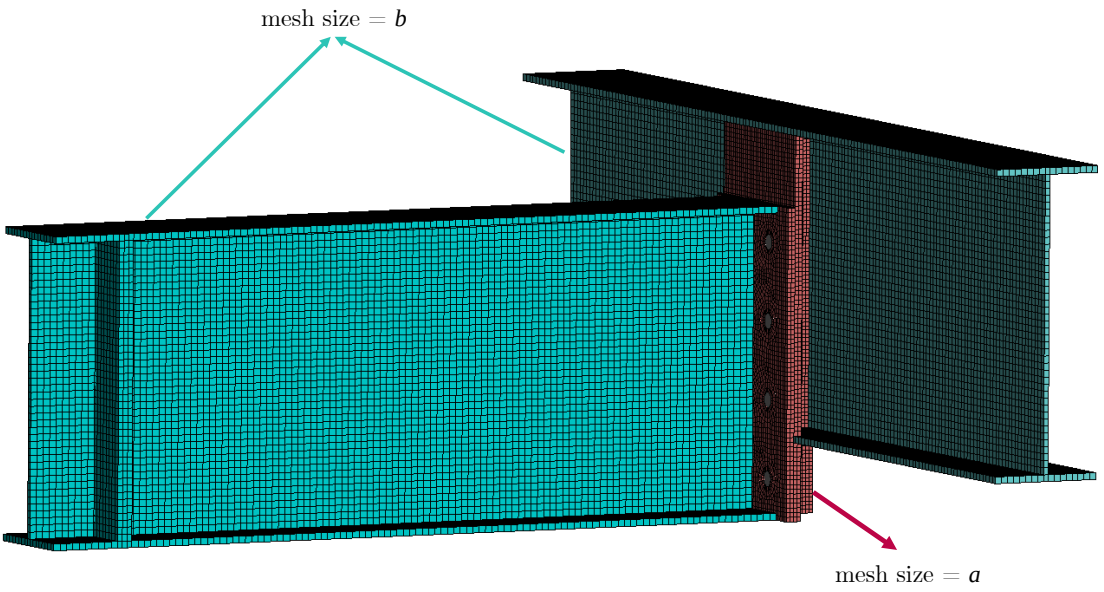

Figure 4.9 Mesh size effect

Table 4.2 lists the mesh size parameters that were employed in the mesh convergence investigation.

Table 4.2 Mesh sizes

Mesh Description	a [mm]	b [mm]
coarse	10	18
medium	7.5	13.5
fine	5	9
very fine	3	9

Fig. 4.10 displays the outcomes of the mesh convergence investigation.

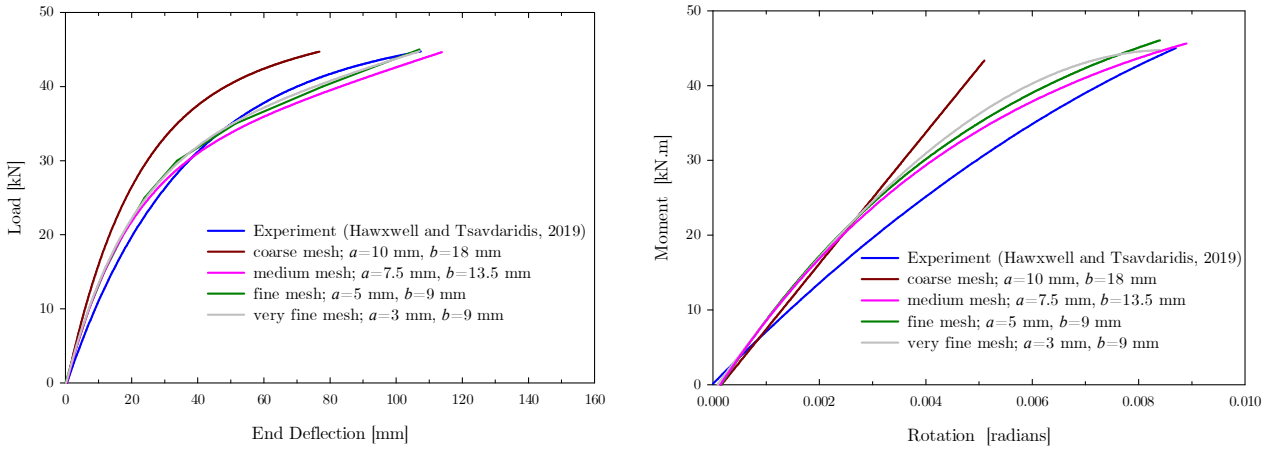

Figure 4.10 Element size effect

Results for this section are tabulated as follows. (see Tables 4.3 and 4.4)

Table 4.3 Rotation during 40 kN according to mesh variation

Experiment [radians] [2]	Mesh Description	Error [radians]	% Error Percentage
7.2×10^{-3}	coarse	4.7×10^{-3}	34.7
	medium	6.7×10^{-3}	7
	fine	6.2×10^{-3}	13.8
	very fine	6.2×10^{-3}	13.8

Table 4.4 Deflection during 40 kN according to mesh variation

Experiment [mm][2]	Mesh Description	Error [mm]	% Error Percentage
74	coarse	52.6	29
	medium	86.4	15.4
	fine	78.6	5.1
	very fine	78.7	5.1

A benchmark point was used for each graph as a baseline outcome to compute the error percentage. Findings for moment vs. rotation (see Table 4.3) indicate that the medium mesh type may be more effective in terms of accuracy and time cost. Yet, it is clear that the 'fine' or 'very fine' mesh emerges when load vs. end deflection findings (see Table 4.4) are taken into consideration. Thus, the 'fine' mesh is chosen to speed up processing. Elements and nodes quantity are around 41.200 and 264.800 respectively, using the 'fine' mesh size.

5. PREPARATION of the FE MODEL

Finite element analysis preparation along with validation of it against the experiment and parameters that are the subject of this study is going to be described in detail, in this section.

5.1. Verification of FEA

For the purpose of comparing experimental data with finite element analysis outcomes, following graphs are utilized. These graphs are shown in Fig. 5.1 and 5.2, respectively.

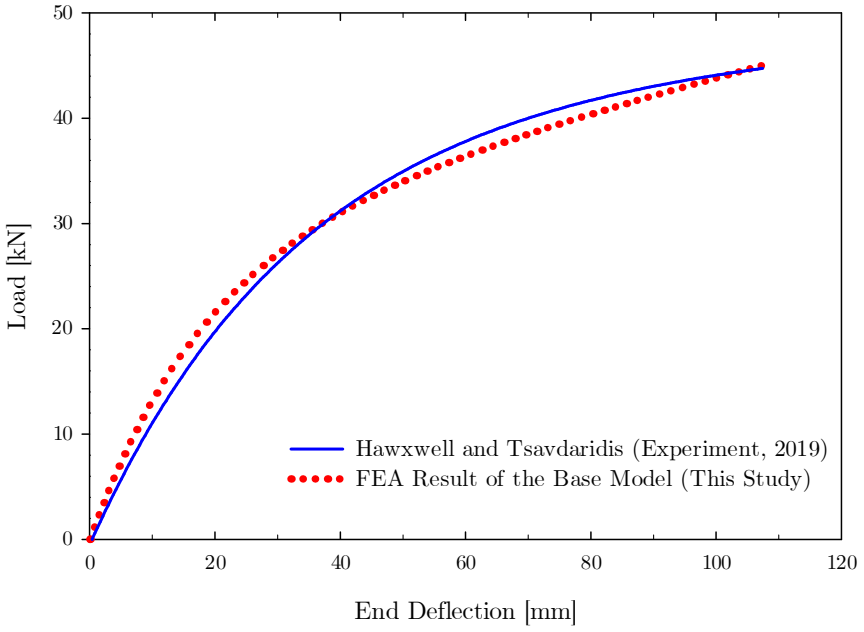

Figure 5.1 Comparison of FEA and experiment, load vs. end deflection

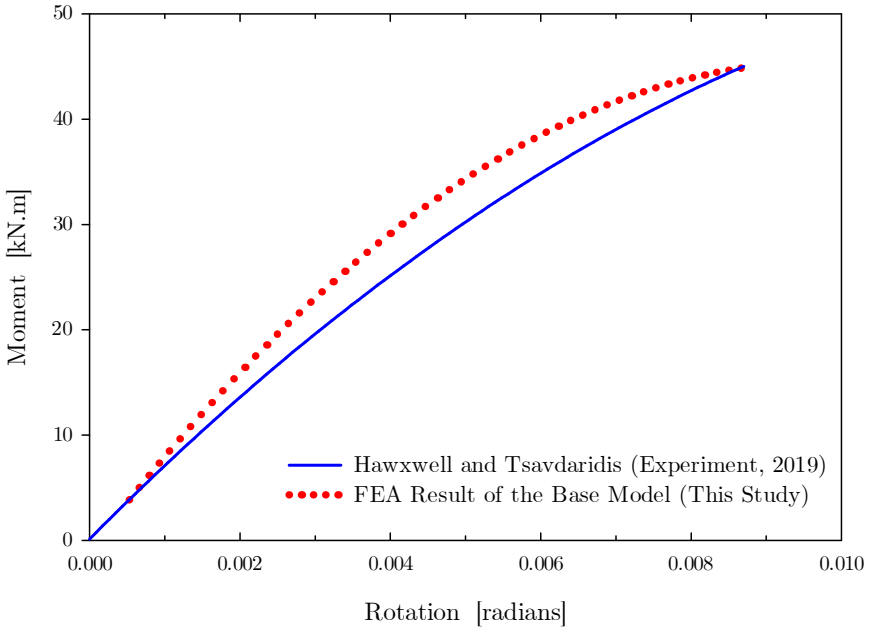

Figure 5.2 Comparison of FEA and experiment, moment vs. rotation

The experiment and FE findings show good convergence, resulting in an accurate and trustworthy FE model. Figures 5.3, and 5.4 depict that consistent results obtained from the FE model.

(a)

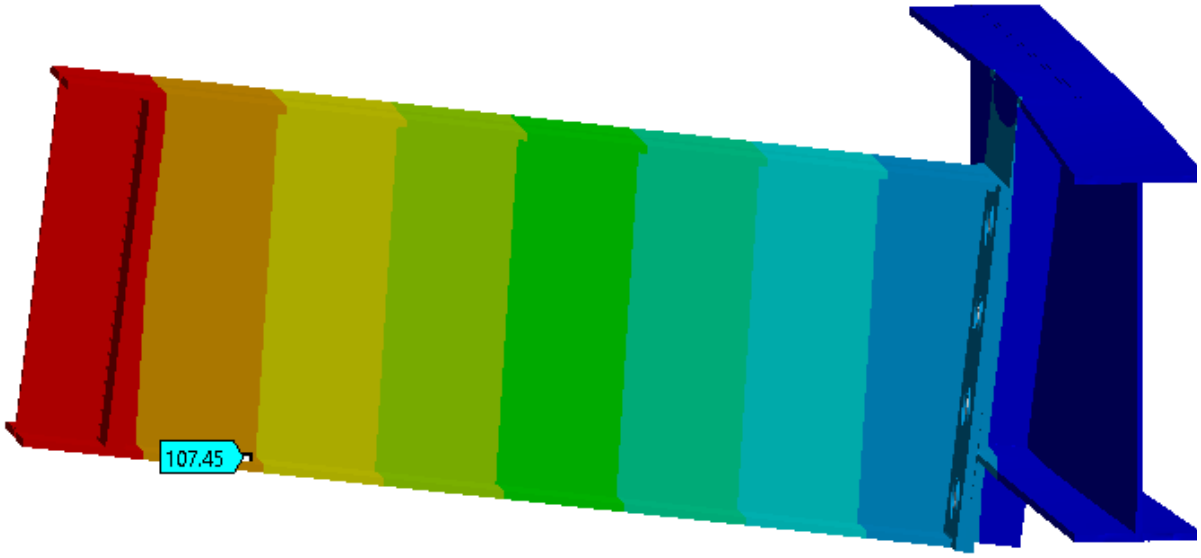

(b)

Figure 5.3 Visual comparison of: a) experiment b) FE model

(a)

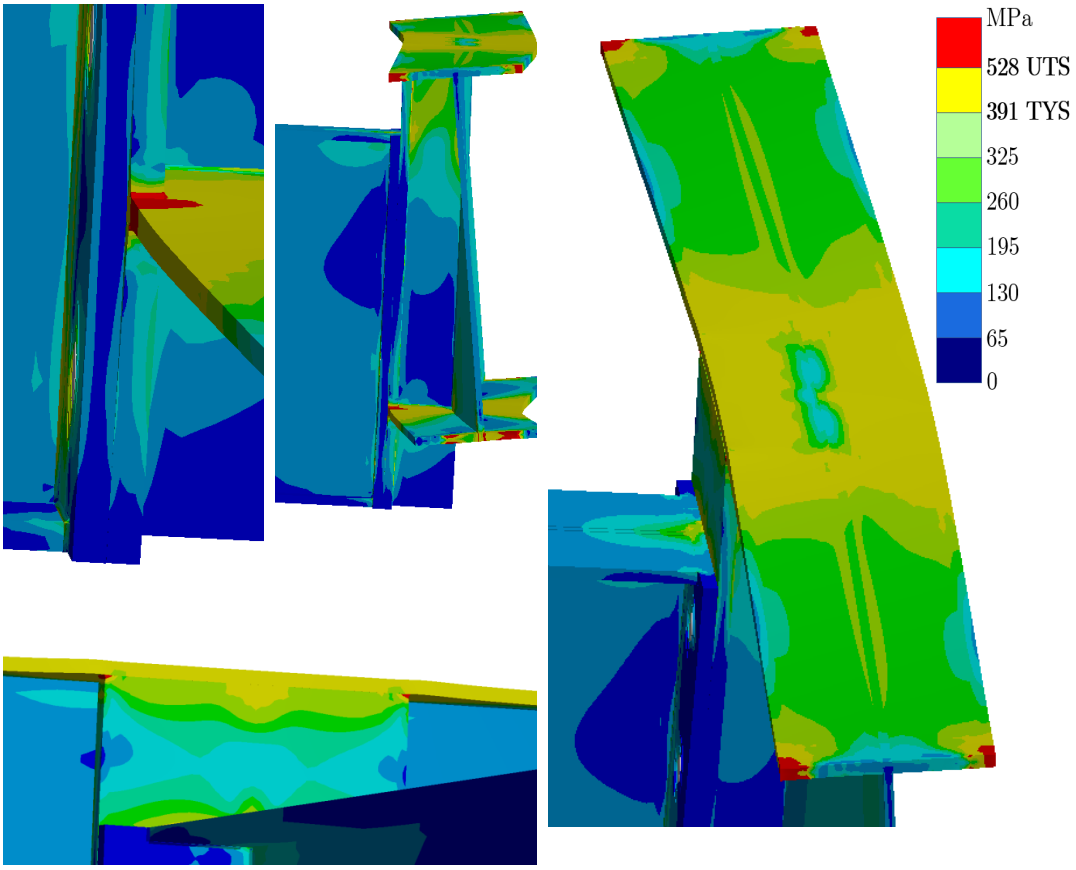

(b)

Figure 5.4 Visual comparison of: a) experiment b) FE model at 43 kN loading

Vertical deflection for the maximal rotation is approximately 107 mm, which corresponds to 43 kN for the base model (see Fig. 5.3). During this greatest load, Figure 5.4 compares the failure mechanisms detected in the test with the findings observed from the FEA model. Results imply that the primary beam rotated excessively, resulting in local deformation on the joint side of the primary beam flange.

5.2. Parametric Study

Experiments are carried out for base model. Several parameters' influences on connection behavior is to get a thorough comprehension of its nature. Validated FE model will henceforth be referred to as the base model because it functions as the foundation for the parametric study. Generally, two phases are involved in the steel structures, frame design and joint design; as a result, the numerous parameters are separated into following groups.

1. Parameters related to frame design:
    - secondary beam section size; S_{sb} = 406×140×39UB (Base Model), 406×140×46UB, 406×140×53UB, 406×178×54UB, 406×178×60UB, 406×178×67UB, 406×178×74UB, 406×178×85UB
    - level inequality of beams; $h =$ from -200 to 200 mm (in 100 mm increments)
    - span length of the secondary beam; 1 m $< L_{sb} <$ 12 m
2. Parameters related to joint design:
    - stiffener plate thickness; $t_1 = 6, 8, 10, 12, 15, 20$ mm
    - end plate thickness; $t_2 = 6, 8, 10, 12, 15, 20$ mm
    - sort of the EEP: fully or partially depth primary end plate
    - bolt quantity

First category identifies connection's characteristics for some beam configurations, which usually comes from frame design. In contrary, second category examines influences of

modifying joints and design of components. Table 5.1 contains a set of parameters and their related values which are covered in this investigation.

Table 5.1 Parametric Study Table

Parameters
Various thicknesses of stiffeners (t_1) in [mm]
6 / 8 / 10 / 12 / 15 / 20
Various thicknesses of end plates (t_2) in [mm]
6 / 8 / 10 / 12 / 15 / 20
Various lengths of the secondary beam (L_{sb})
1 m to 12 m in 1 m increments
Section sizes of the secondary beam (S_{sb}) in [mm]
406×140×39UB
406×178×54UB
406×178×60UB
406×178×67UB
406×178×74UB
406×178×85UB
Section sizes of the primary beam (S_{pb}) in [mm]
406×140×39UB
406×140×53UB
406×178×54UB
406×178×85UB
Level inequality of the beams h in [mm]
-200 / -100 / 0 / +100 / +200
End plates
FDPEP
PDPEP
Eliminating bolts
Eliminating of Second Bolt Row
Eliminating of Third Bolt Row
Including all bolts

In the subsequent section, influences of previously mentioned parameters will be analyzed in detail. In addition, failure mechanisms and corresponding failure zones will be explained. For all parameters moment values that given in the figure captions are the strength capacity which indicates that at this moment value ultimate strength value of S355 steel is observed.

6. RESULTS AND DISCUSSION

6.1. Stiffener thickness influence, t_1

As seen in Fig. 6.1, analyses revealed three conspicuous failure regions. Zone 1 in Fig. 6.1a is the bottom of the lower stiffener. Fig. 6.1b depicts Zone 2 as the upper region of end plate surrounding upper fasteners. And lastly, Zone 3, depicted in Fig. 6.1b is a region where secondary end plate apply pressure to the primary end plate.

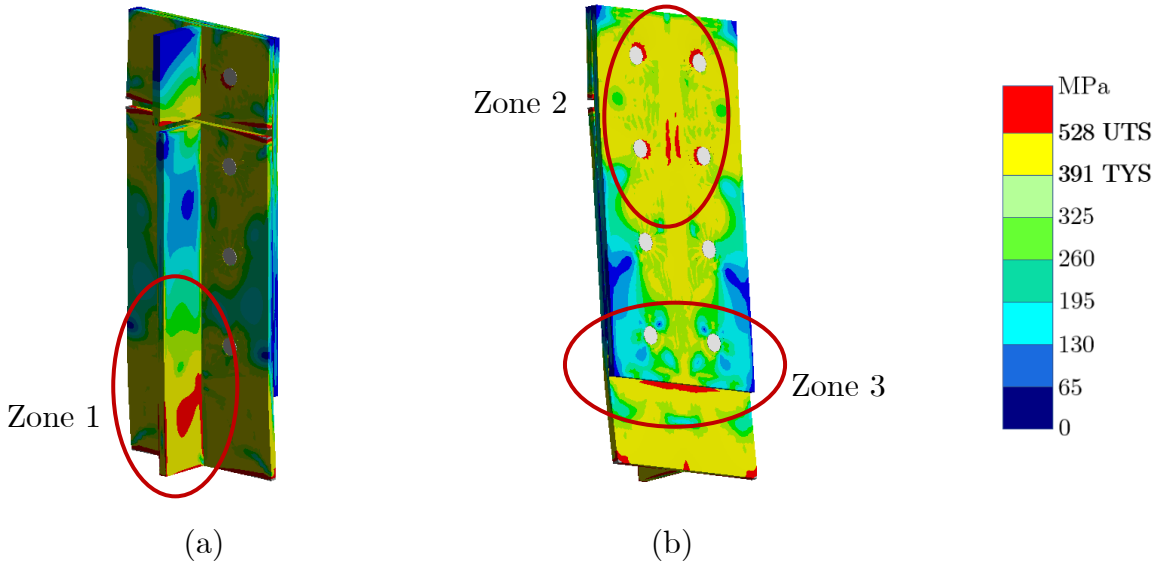

Figure 6.1 Failure mechanism zones; distribution patterns of the equivalent stress : a) back view, b) front view; (M = 80 kN.m, t_1 = 10 mm, t_2 = 8 mm, L_{sb} = 1 m, S_{sb} = 406×140×39UB, h = 0 mm)

Figure 6.2 depicts the equivalent stresses of the joint depending on the stiffener thicknesses denoted as t_1 (See Fig. 4.2). Results obtained for the range from 6 to 12 mm led to this comment; Zone 1 yields first as force increases to higher values.

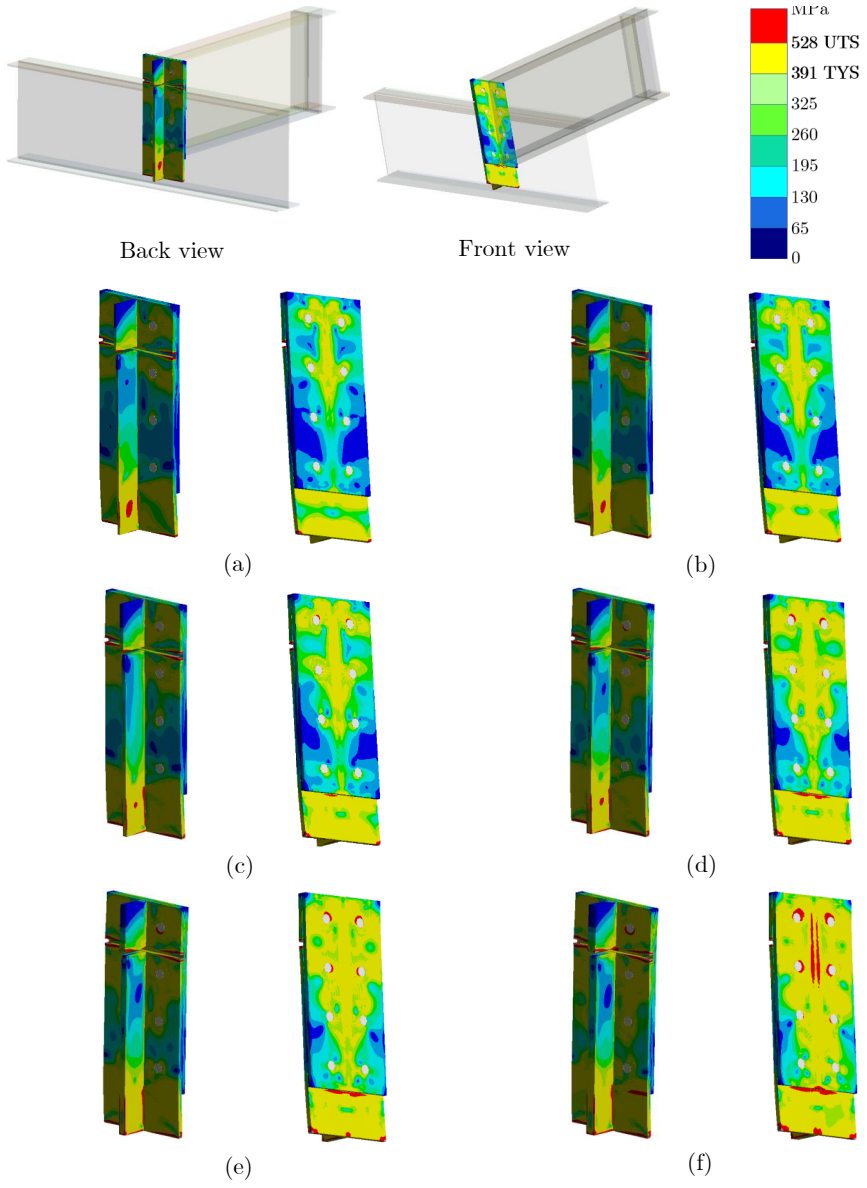

Figure 6.2 Back view Influence of the stiffener thickness, distribution patterns of the equivalent stress near the primary beam to secondary beam connection: a) $t_1 = 6$ mm, $M = 65$ kN.m, b) $t_1 = 8$ mm, $M = 76$ kN.m, c) $t_1 = 10$ mm, $M = 85$ kN.m, d) $t_1 = 12$ mm, $M = 100$ kN.m, e) $t_1 = 15$ mm, $M = 115$ kN.m, f) $t_1 = 20$ mm, $M = 140$ kN.m; ($t_2 =$ 10 mm, $L_{sb} = 1$ m, $S_{sb} = 406\times140\times39$UB, $h = 0$ mm)

Zone 3 turns into the failure area for stiffeners thicker than 12 mm, where the primary end plate is exposed to pressure from the secondary end plate. As stiffeners thickens, the height/thickness ratio (slenderness) declines, restraining the stiffener from experiencing local deformation effects. Consequently, the region of failure shifts toward the end plates.

Figure 6.3 depicts the moment-rotation results, and Table 6.1 lists the failure areas with respect to the thickness variation. The simulation concludes for each case as a connection part experiences its ultimate tensile strength. As a finding from this graph, thicker stiffeners increase the moment capacity of the secondary beam, while thinner stiffeners cause greater rotation for a fixed moment than thicker stiffeners.

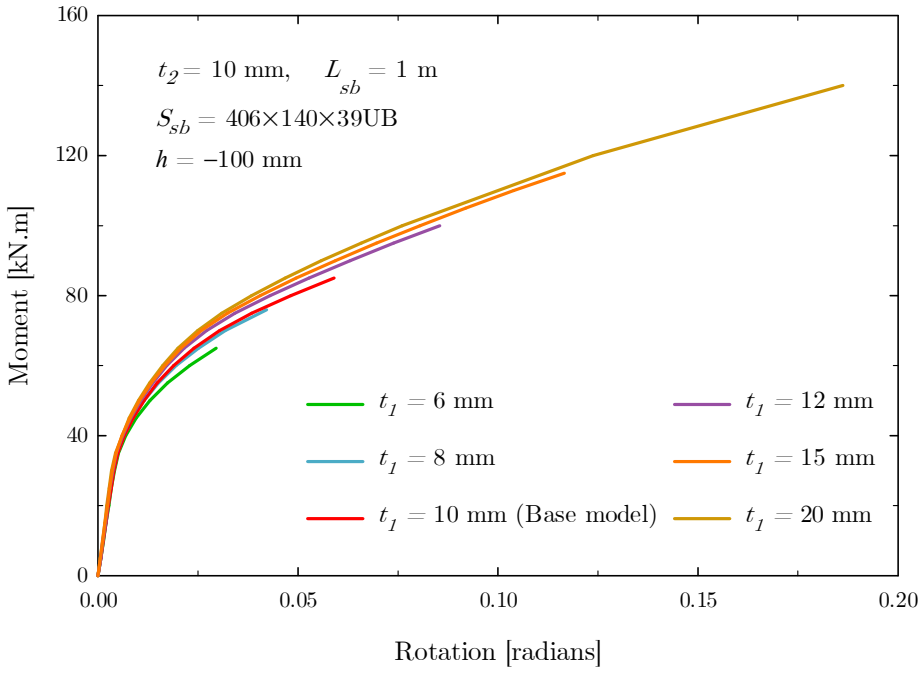

Figure 6.3 Influence of t_1

Table 6.1 Failure regions according to stiffener thickness variation

t_1 **(mm)**	**Figures**	**Failure Mechanism Zones**
6	Fig. 5.3a	Zone 1
8	Fig. 5.3b	Zone 1
10	Fig. 5.3c	Zone 1, 3
12	Fig. 5.3d	Zone 1, 2, 3
15	Fig. 5.3e	Zone 2, 3
20	Fig. 5.3f	Zone 2, 3

6.2. Effect of the thickness of end plates, t_2

The response of increasing end plate thickness is investigated by adjusting this parameter from 6 to 20 mm. Figure 6.4 depicts the equivalent stresses of the joint.

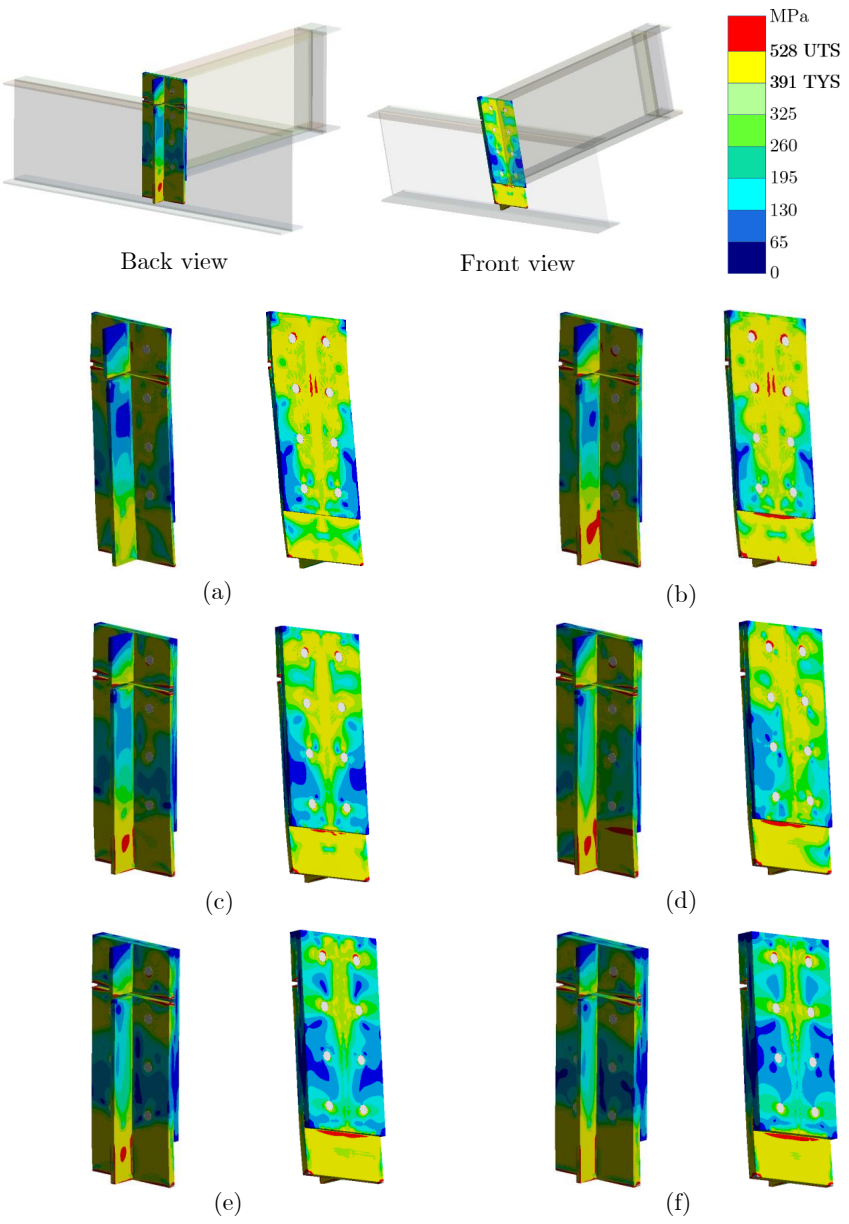

Figure 6.4 Influence of the end plate thickness, distribution patterns of the equivalent stress: a) $t_2 =$ 6 mm, $M = 55$kN.m, b) $t_2 = 8$ mm, $M = 80$ kN.m, c) $t_2 = 10$ mm, $M = 85$ kN.m, d) $t_2 = 12$ mm, $M = 102$ kN.m, e) $t_2 = 15$ mm, $M = 110$ kN.m, f) $t_2 = 20$ mm, $M = 140$ kN.m; ($t_1 = 10$ mm, $L_{sb} = 1$ m, $S_{sb} = 406\times140\times39$UB, $h = 0$ mm)

Thin-walled steel members are regarded to have a 6 mm thickness, yet it is studied for comparison intents. Joint with 6 mm thickness seems to be the weakest joint among all

as expected, and failure occurs first on the end plate itself. In Zones 1 and 3, however, there are no stresses that would lead to failure. Figure 6.4 depicts the equivalent stress pattern at loading for t_2 =8 mm. In this instance, yielding occurs in all zones. At the loading that causes failure for t_2 =10 mm, t_2 =12 mm, and t_2 =15 mm, the tension amount in Zone 2 decreases, and Zone 1 and Zone 3 are determined to be the failure zones. As depicted in Fig. 6.4f, the thickest end plate exhibits entirely distinct performance characteristics, with failure occurring only in Zone 3. Table 6.2 outlines the failure zone variation according to end plate thickness.

Table 6.2 Failure regions according to end plate thickness variation

t_2 **(mm)**	**Figures**	**Failure Mechanism Zones**
6	Fig. 6.4a	Zone 2
8	Fig. 6.4b	Zone 1, 2, 3
10	Fig. 6.4c	Zone 1, 3
12	Fig. 6.4d	Zone 1, 3
15	Fig. 6.4e	Zone 1, 3
20	Fig. 6.4f	Zone 3

As the component's slenderness increases (thickness decreases), the ineffective compressive areas broaden, resulting in a decrease in moment capacity. In addition, the stresses on the secondary end plate decrease gradually as the moment applied to the connection increases from Fig. 6.5a to 6.5f. In Fig. 6.6, the effect of end plate thickness change is presented as a multi-line graph.

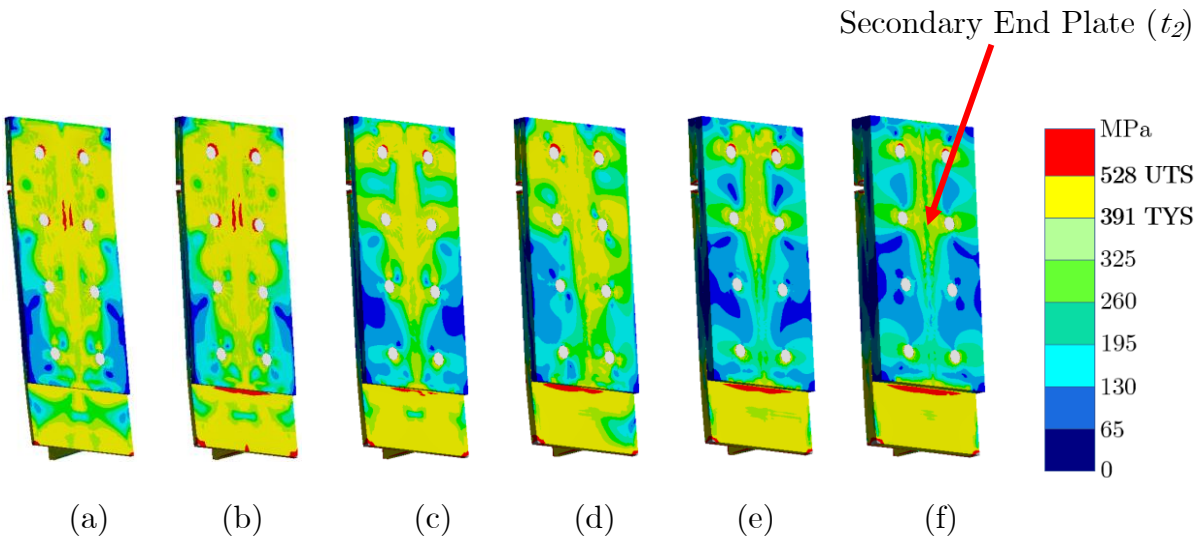

Figure 6.5 Distribution patterns of the equivalent stress: a) $t_2 = 6$ mm, $M = 55$kN.m, b) $t_2 = 8$ mm, $M = 80$ kN.m, c) $t_2 = 10$ mm, $M = 85$ kN.m, d) $t_2 = 12$ mm, $M = 102$ kN.m, e) $t_2 = 15$ mm, $M = 110$ kN.m, f) $t_2 = 20$ mm, $M = 140$ kN.m; ($t_1 = 10$ mm, $L_{sb} = 1$ m, $S_{sb} = 406\times140\times39$UB, $h = 0$ mm)

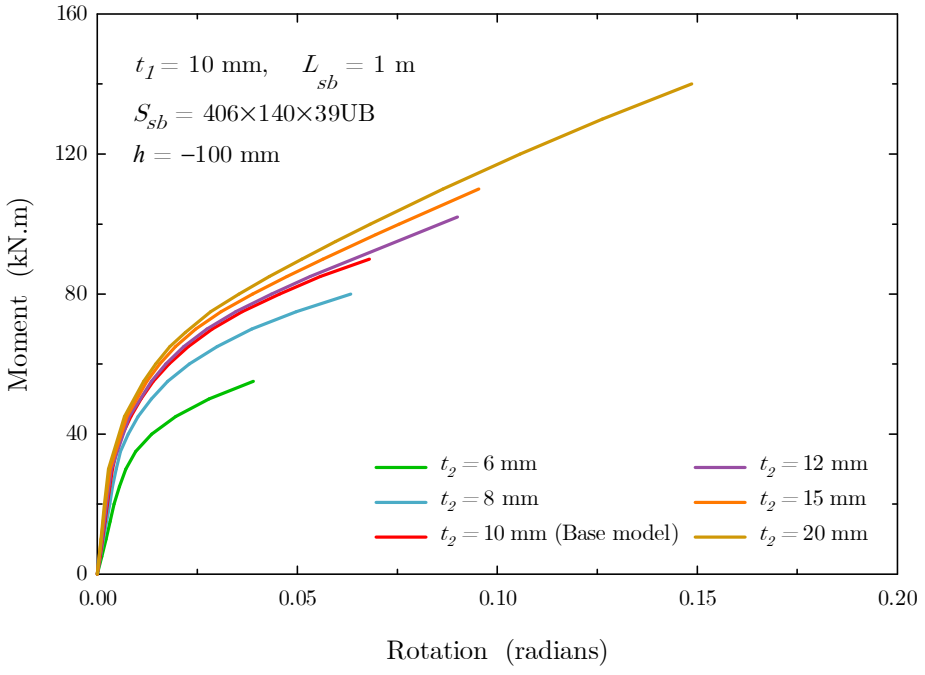

Figure 6.6 End plates' thickness effect

6.3. Effect of secondary beam length, L_{sb}

Secondary beam's length, L_{sb}, is a crucial specification which influences the initial stiffness boundary of the connection and affects joint strength classification. Initial stiffness boundaries ($S_{j.ini}$) of the beams are calculated for the common steel structure application range of L_{sb} =1 m to 12 m. $S_{j.ini}$ is determined using the BS EN 1993-1 [3] as:

$$S_{j.ini} = \frac{EI_b}{2L_{sb}}, \tag{4}$$

where I_b is the second moment of area of the secondary beam (0.000125 m^4) and E is the modulus of elasticity (210 GPa). Two parameters can typically be used to classify the strength of joints: initial stiffness and moment capacity. The classification according to the initial stiffness variation of various lengths are listed in Table 6.3, and the initial slopes of moment-rotation curves are shown in Fig. 6.7.

Table 6.3 Initial Stiffness Values for Different Spans (L_{sb})

Length [m]	S_j **[kN.m/rad]**	**Moment [radians]**	**Stiffness Classification**
1	13125.00	0.0049	Nominally-Pinned
2	6562.50	0.0098	Semi-Rigid
3	4375.00	0.0147	Semi-Rigid
4	3281.25	0.0196	Semi-Rigid
5	2625.00	0.0245	Semi-Rigid
6	2187.50	0.0294	Semi-Rigid
7	1875.00	0.0343	Semi-Rigid
8	1640.63	0.0392	Semi-Rigid
9	1458.33	0.0441	Semi-Rigid
10	1312.50	0.0490	Semi-Rigid
11	1193.18	0.0538	Semi-Rigid
12	1093.75	0.0587	Semi-Rigid

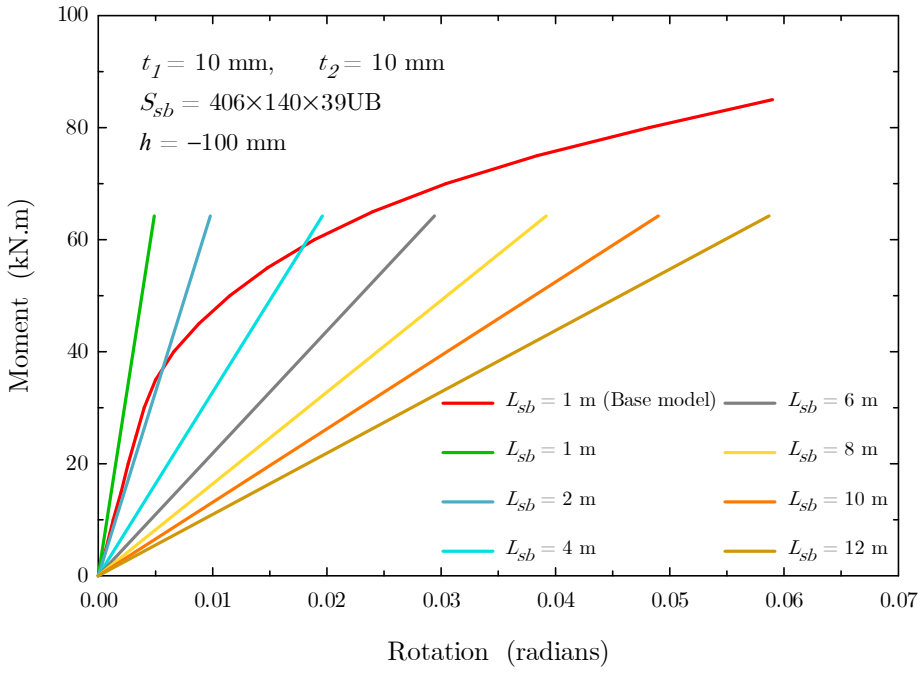

Figure 6.7 Effect of secondary beam length

As secondary beams become shorter (or L_{sb} decreases), the slope, $S_{j.ini}$, increases, according to Fig. 6.7. Consequently, the possibility that the joints are classified as flexible increases.

6.4. Effect of the Secondary Beam Section Size, S_{sb}

Connection classification can be made by its design moment resistance. A joint will be counted as flexible if its moment response to loading is lower than 0.25 times M_{Rd} [3]. Change of section sizes doesn't effect response of the joint against loading remarkably. However, this variation affect classification initial boundary due to M_{Rd} change. Various section size values and corresponding M_{Rd} values [28] along with joint classifications are tabulated in Table 6.4.

Table 6.4 S_{sb} vs. Stiffness Classification

Section Size	M_{Rd} **[kN.m]**	**0.25** $\times$ M_{Rd} **[kN.m]**	**Stiffness Classification**
406×140×39UB	256	65	Semi-Rigid
406×140×46UB	314	79	Semi-Rigid
406×140×53UB	365	92	Flexible
406×178×54UB	372	94	Flexible
406×178×60UB	425	107	Flexible
406×178×67UB	478	120	Flexible
406×178×74UB	532	134	Flexible
406×178×85UB	596	150	Flexible

The classification of the joints is determined through assessing both Table 6.4 and Fig. 6.8 together.

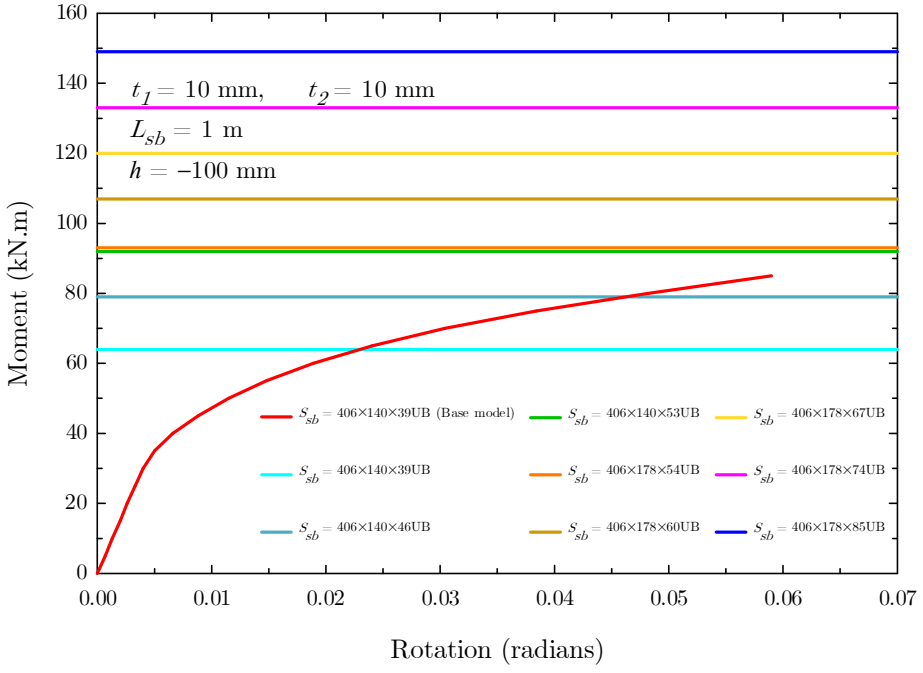

Figure 6.8 Effect of S_{sb}

Variation in dimensions of the section size and length of the beams does not affect the behavior of the base model joint since beams are not a component of the joint. Yet, change of the section size or length of the beam directly shifts boundaries that determine the joint's stiffness classification. As shown in Fig. 6.8 the initial boundaries are relatively higher when looking larger section sizes, indicating that more rigid joints may used for larger beams. This suggests that the design of joints should be carefully considered based on the size of the beam to assure that the convenient grade of ductility is achieved.

6.5. Effect of Level Inequality of Beams, h

There can be a level nonalignment between primary and secondary beams in steel structures due to architectural considerations. To determine the impact of this variant, five distinct beam levels (from -200 to 200 mm in 100 mm increments) are studied. Negative values indication of h is shown in Fig. 6.9.

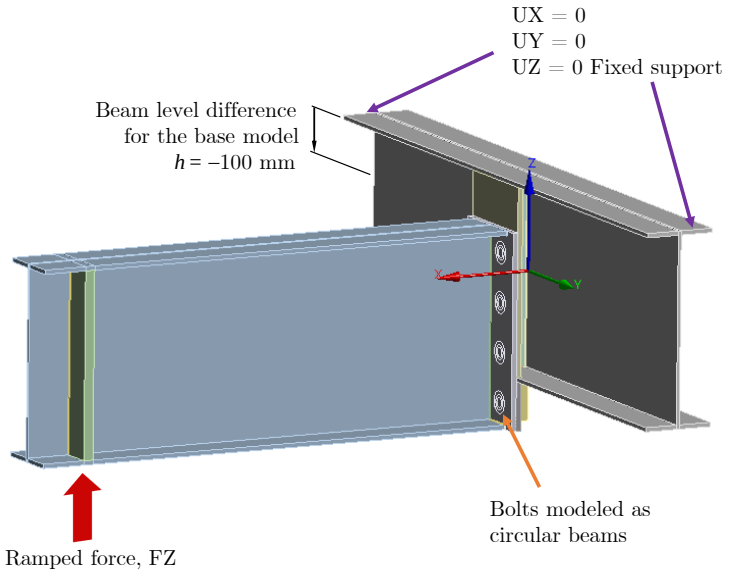

Figure 6.9 Boundary conditions with applied load

Figure 6.10 illustrates the findings of the moment-rotation characteristic associated with beams' level difference. In the case where h equals zero, the stiffest behavior is experienced.

The initial slope as well the moment capacity diminish as the level inequality between end plates increases. This indicates that the stiffness of the connection decreases when level inequality of end plates increases. Findings suggest that designing connections with minimal level differences can improve their overall stiffness and moment capacity.

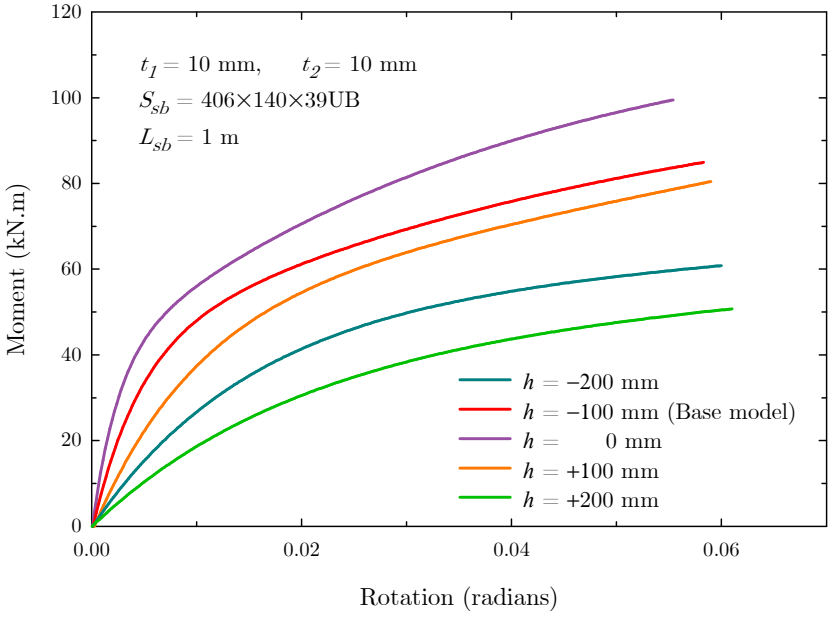

Figure 6.10 Effect of inequality in level of beams

In situation where h equals to zero the most rigid action is observed. Initial slope as well as moment capacity diminish as level inequality between the beams rises ($|h| > 0$). When the level inequality of beams rises it is obviously understood rotation amount increases. On the other hand, comparing levels that has same absolute value, minus levels develop more rotation. This is because due to the level inequality sign (minus or plus) stiffeners location change. For the positive values, stiffeners shift from tension zone to the compression zone according to loading and make contribution to the secondary beam resistance to rotation and this situation decreases rotation. It can be interpreted from these results that as the level inequality of the end plates raises, possibility of the connection to be classified as flexible

increases. Equivalent stress patterns occurred by changing this parameter is shown in Fig. 6.11.

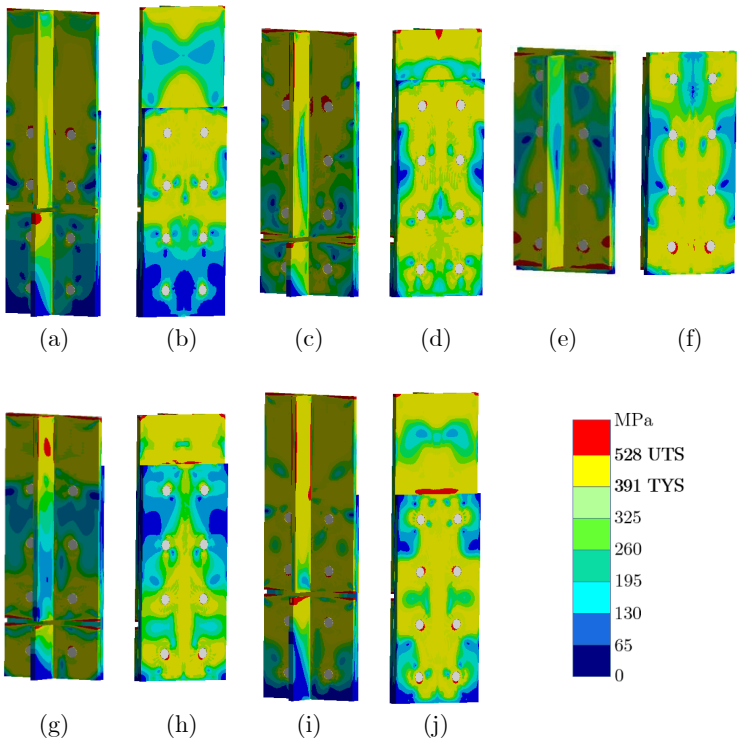

Figure 6.11 Distribution patterns of the equivalent stress: a,b) $h = -200$ mm c,d) $h = -100$ mm e,f) $h = 0$ mm g,h) $h = 100$ mm i,j) $h = 200$ mm ($t_1 = 10$ mm, $t_2 = 10$ mm, $L_{sb} = 1$ m, $S_{sb} = 406\times140\times39$UB)

6.6. Effect of PDPEP

The initial design is a fully depth primary end plate which consists of a plate that weld across the primary beam's flanges. Another option that can be alternative of FDPEP is to construct a partially depth primary end plate. For the PDPEP connections, top surface of end plate is welded to primary end plate top flange, whereas bottom surface of the end plate remains in some depth and does not reach until the primary beams' opposite flange (see the sketch in Fig. 6.12).

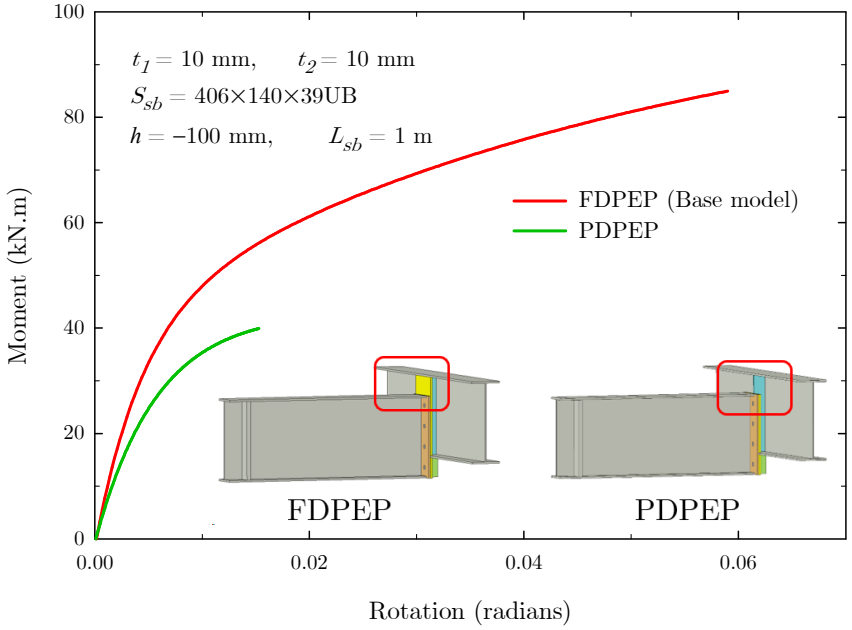

Figure 6.12 Comparison of PDPEP vs. FDPEP

Figures 6.12 and 6.13, compares FDPEP and PDPEP, both in terms of response of joints against loading and generated equivalent stress values.

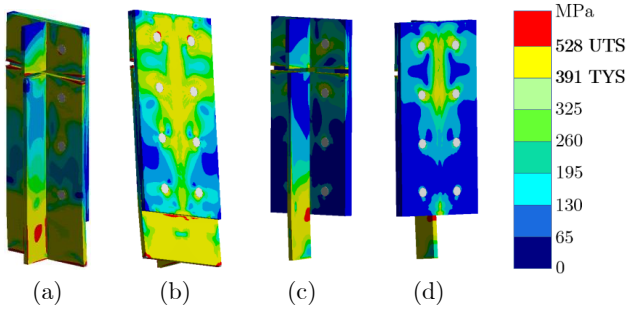

Figure 6.13 Distribution patterns of equivalent stress: a) FDPEP, M = 85 kN.m, back view, b) FDPEP, M = 85 kN.m, front view c) PDPEP, M = 40 kN.m, back view d) PDPEP model, M = 40 kN.m, front view; (t_1 = 10 mm, t_2 = 10 mm, L_{sb} = 1 m, S_{sb} = 406×140×39UB), h = +100 mm

As a finding of this analysis, PDPEP developed more rotation than FDPEP, and experienced the ultimate strength first. Because as a weak point partial plate cause pressure on the lower stiffener contact surface and finally initiating the failure. Both according to initial stiffness

and observing the ultimate tensile strength partial depth primary end plate remains under the full depth primary end plate which make it relatively weaker connection type.

6.7. Effect of Eliminating Some Bolts

The first design consists of four rows of fasteners with two bolts per row. This part examines the influence of reducing the number of fasteners on the joint characteristics. Due to the minimum requirement that the first and fourth rows of fasteners exist, the second and third rows were removed for the analysis. As shown in Fig. 6.14, eliminating of Bolt Row 2 caused a slight decrease in the initial rigidity.

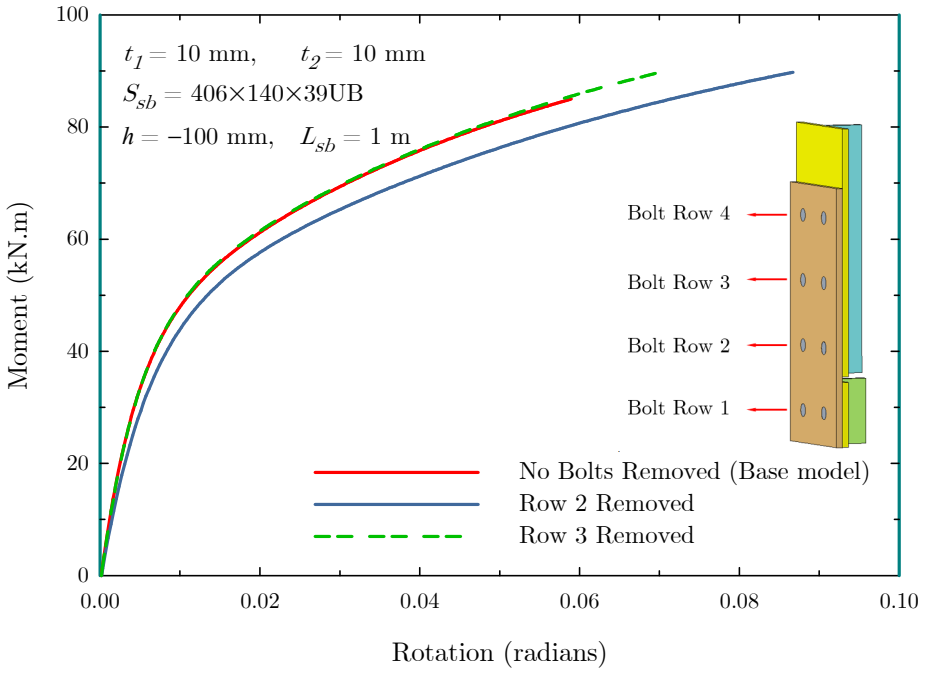

Figure 6.14 Effect of eliminating some bolt rows

As understood by these results, loading to the joint causes compression in the lower side, conversely tension in the bolts, so removing of second row is going to have a greater influence than removing third row. However, when considered in general, the elimination of the second

and third fastener rows has a negligible impact on joint's initial rigidity as well as moment strength.

7. CONCLUSION

For accurate evaluation and construction of steel joints, it is necessary to comprehend the response of the joints against loading and accordingly classify them accurately. Size and geometry of connecting components and beams significantly influence joint categorization. This parametric analysis shows the limitations for the beam-to-beam connections' classification to be made properly for a variety of critical factors.

- As the end plate thickness increased, in spite of increasing loading capacity of the joint, stresses decrease gradually on the secondary end plate. Instead, stress concentration shifts towards the area that secondary end plate implements pressure onto primary end plate.
- The span of the secondary beam length directly affects the initial stiffness boundary. Since, shorter secondary beams do not rotate as much as longer beams do, initial stiffness boundary gets increased for shorter beams. Therefore, the connection classification is likely to be nominally pinned for shorter beams and semi rigid for longer beams.
- With buckling in the flange, primary beam seems as a critical part which causing failure.
- Stiffeners used in the joints that has level difference contribute more resistance to the connection when they positioned in the tension zone comparing to the compression zone.
- When level inequality between beams raised, initial stiffness as well as joint strength decreases.
- Eliminating bolt rows has little impact on joints' initial rigidity and strength capacity.

REFERENCES

[1] Jean-Pierre Jaspart. General report: session on connections. *Journal of Constructional Steel Research*, 55(1-3):69–89, **2000**.

[2] Daniel Allan Hawxwell and Konstantinos Daniel Tsavdaridis. Beam-to-beam eccentric end plate connections-Experimental comparison to fin plate and partial-depth end plate connections. *Structures*, 19:411–423, **2019**.

[3] British Standard. Eurocode 3—design of steel structures—. *BS EN 1993-1*, 1:2005, **2006**.

[4] Hao Wang, Bo Yang, Xu-Hong Zhou, and Shao-Bo Kang. numerical analyses on steel beams with fin-plate connections subjected to impact loads. *Journal of Constructional Steel Research*, 124:101–112, **2016**.

[5] Ying Zhang, Shan Gao, Lanhui Guo, Jiayi Qu, and Sheliang Wang. Ultimate tensile behavior of bolted T-stub connections with preload. *Journal of Building Engineering*, 47:103833, **2022**.

[6] Mohammad Jobaer Hasan, Mahmud Ashraf, Safat Al-Deen, Sukanta Kumer Shill, and Brian Uy. Stainless steel top-seat angle beam-to-column connection: Full-scale test and analytical modelling. In *Structures*, volume 34, pages 4322–4338. Elsevier, **2021**.

[7] Xuesen Chen and Gang Shi. Experimental study on seismic behaviour of cover-plate joints in high strength steel frames. *Engineering Structures*, 191:292–310, **2019**.

[8] Yasin Onuralp Özkılıç and Cem Topkaya. Extended end-plate connections for replaceable shear links. *Engineering Structures*, 240:112385, **2021**.

[9] Manuel Lopez, Alfonso Loureiro, Ruth Gutierrez, and Jose M Reinosa. A new analytical formulation for the stiffness and resistance of the additional plate in bending in beam-to-beam steel joints. *Engineering Structures*, 228:111476, **2021**.

[10] Kestutis Urbonas and Alfonsas Daniūnas. Behaviour of semi-rigid steel beam-to-beam joints under bending and axial forces. *Journal of constructional steel research*, 62(12):1244–1249, **2006**.

[11] Vijayakumar Natesan and Mahendrakumar Madhavan. Performance of CFS beam-to-beam bolted connection using clip angle and flange strip: Experimental investigation. *Journal of Structural Engineering*, 145(10):04019101, **2019**.

[12] MR Mohamadi-Shooreh, M Mofid, and SL McCabe. Empirical model of the moment-rotation curve of beam-to-beam bolted flush endplate connections. *Journal of Structural Engineering*, 139(1):66–72, **2013**.

[13] BS EN 1993-1-8: 2005. Design of steel structures-part 1-8: design of joints. **2005**.

[14] MA Hadianfard and R Razani. Effects of semi-rigid behavior of connections in the reliability of steel frames. *Structural Safety*, 25(2):123–138, **2003**.

[15] LMC Simoes. Optimization of frames with semi-rigid connections. *Computers & structures*, 60(4):531–539, **1996**.

[16] Merve Sağıroğlu, Mahyar Maali, Mahmut Kılıç, and Abdulkadir Cüneyt Aydın. A novel approach for bolted T-stub connections. *International Journal of Steel Structures*, 18(3):891–909, **2018**.

[17] Rohola Rahnavard, Navid Siahpolo, Mohammad Naghavi, and Akbar Hassanipour. Analytical study of common rigid steel connections under the effect of heat. *Advances in Civil Engineering*, 2014, **2014**.

[18] WG Altman, A Azizinamini, JH Bradburn, and JB Radziminski. *Moment-rotation characteristics of semi-rigid steel beam-column connections*. National Technical Information Service, **1983**.

[19] David Anderson and Zoubir Benterkia. Analysis of semi-rigid steel frames and criteria for their design. *Journal of Constructional Steel Research*, 18(3):227–237, **1991**.

[20] Miklos Ivanyi. Semi-Rigid Joints Instructural Steelwork. **2000**.

[21] A Bahaz, S Amara, Jean-Pierre Jaspart, and Jean-François Demonceau. Analysis of the behaviour of semi rigid steel end plate connections. In *MATEC Web of Conferences*, volume 149, page 02058. EDP Sciences, **2018**.

[22] Vitor Rodrigues Gomes, André Tenchini, Luciano Lima, and Pedro Vellasco. Robustness assessment of semi-rigid steel multi-storey frames. In *Structures*, volume 25, pages 849–860. Elsevier, **2020**.

[23] Rasha K Al-Fisalawi, AL-Hadithy Laith Khalid, and Mustafa Kamal Al-Kamal. Performance of semi-rigid steel connections under monotonic and cyclic loadings: a review. In *IOP Conference Series: Materials Science and Engineering*, volume 1067, page 012059. IOP Publishing, **2021**.

[24] F Iannone, M Latour, V Piluso, and G Rizzano. Experimental analysis of bolted steel beam-to-column connections: component identification. *Journal of Earthquake engineering*, 15(2):214–244, **2011**.

[25] A Loureiro, A Moreno, R Gutiérrez, and JM Reinosa. Experimental and numerical analysis of three-dimensional semi-rigid steel joints under non-proportional loading. *Engineering Structures*, 38:68–77, **2012**.

[26] Ali Köken and Mehmet Alpaslan Köroğlu. Experimental study on beam-to-column connections of steel frame structures with steel slit dampers. *Journal of Performance of Constructed Facilities*, 29(2):04014066, **2015**.

[27] Jinming Zeng, Wei Lu, and Juha Paavola. Ultimate strength of a beam-to-column joint in a composite slim floor frame. *Journal of Constructional Steel Research*, 140:82–91, **2018**.

[28] Tata Steel Europe Ltd. *Tata Steel Section Interactive Blue Book*. **2015**.